Paxillin Phosphorylation Controls Invadopodia/Podosomes Spatiotemporal Organization.

Cédric Badowski, Géraldine Pawlak, Alexei Grichine, Anne Chabadel, Christiane Oddou, Pierre Jurdic, Martin Pfaff, Corinne Albiges-Rizo, Marc Block

Molecular Biology of the Cell
Vol. 19, 633–645, February 2008

Paxillin Phosphorylation Controls Invadopodia/Podosomes Spatiotemporal Organization

Cédric Badowski,*† Géraldine Pawlak,*† Alexei Grichine,†‡ Anne Chabadel,§ Christiane Oddou,*† Pierre Jurdic,§ Martin Pfaff,*† Corinne Albigès-Rizo,*† and Marc R. Block*†

*Equipe DySAD, Institut Albert Bonniot, Institut National de la Santé et de la Recherche Médicale U823, 38042 Grenoble Cedex 09, France; †Université Joseph Fourier, 38041 Grenoble Cedex 09, France; ‡Cell Imaging Platform, Institut Albert Bonniot, Institut National de la Santé et de la Recherche Médicale U823, 38706 La Tronche Cedex, France; and §Ecole Normale Supérieure de Lyon, 69364 Lyon Cedex 07, France

Submitted January 30, 2006; Revised November 5, 2007; Accepted November 19, 2007
Monitoring Editor: Mark Ginsberg

In Rous sarcoma virus (RSV)-transformed baby hamster kidney (BHK) cells, invadopodia can self-organize into rings and belts, similarly to podosome distribution during osteoclast differentiation. The composition of individual invadopodia is spatiotemporally regulated and depends on invadopodia localization along the ring section: the actin core assembly precedes the recruitment of surrounding integrins and integrin-linked proteins, whereas the loss of the actin core was a prerequisite to invadopodia disassembly. We have shown that invadopodia ring expansion is controlled by paxillin phosphorylations on tyrosine 31 and 118, which allows invadopodia disassembly. In BHK-RSV cells, ectopic expression of the paxillin mutant Y31F-Y118F induces a delay in invadopodia disassembly and impairs their self-organization. A similar mechanism is unraveled in osteoclasts by using paxillin knockdown. Lack of paxillin phosphorylation, calpain or extracellular signal-regulated kinase inhibition, resulted in similar phenotype, suggesting that these proteins belong to the same regulatory pathways. Indeed, we have shown that paxillin phosphorylation promotes Erk activation that in turn activates calpain. Finally, we observed that invadopodia/podosomes ring expansion is required for efficient extracellular matrix degradation both in BHK-RSV cells and primary osteoclasts, and for transmigration through a cell monolayer.

INTRODUCTION

Podosomes are dot-like actin-rich structures involved in cell/extracellular matrix (ECM) adhesion found in some specific cell types such as cells belonging to the monocytic lineage including osteoclasts, macrophages, and dendritic cells. They have also been described in aortic endothelial cells (Moreau *et al*., 2003), smooth muscular cells (Gimona *et al*., 2003), and Src-transformed cells (Tarone *et al*., 1985; Marchisio *et al*., 1987; Gavazzi *et al*., 1989; Ochoa *et al*., 2000; Abram *et al*., 2003). In osteoclasts, rosettes also called podosome rings were shown to expand and fuse in a microtubule-dependent manner, leading to the formation of podosome belts localized at the cell periphery (Destaing *et al*., 2003, 2005; Jurdic *et al*., 2006). Due to the oncogenic activity of v-Src, Src-transformed cells are closer to cancer rather than normal cells; thus, their adhesive structures are more related to invadopodia (Linder, 2007). Indeed, invadopodia are protrusions emanating from the ventral surface of invasive cancer cells (Mueller and Chen, 1991; Yamaguchi *et al*., 2005; Gimona and Buccione, 2006) exhibiting a very high proteolytic activity toward the extracellular matrix (Mueller and Chen, 1991; Mueller *et al*., 1992), one aspect that was reported in many articles to be the hallmark these structures (Baldassarre *et al*., 2003; Buccione *et al*., 2004; McNiven *et al*., 2004; Linder and Kopp, 2005; Ayala *et al*., 2006; Gimona and Buccione, 2006; Linder, 2007). Invadopodia of Src-transformed cells were shown to self-organize into rosettes similarly to what was observed for podosomes in osteoclasts (Destaing *et al*., 2003) and endothelial cells (Moreau *et al*., 2003).

Podosomes and invadopodia share many components and structural features (Linder and Aepfelbacher, 2003; Buccione *et al*., 2004; Gimona and Buccione, 2006). They have two distinct parts: the core is an actin-rich column (Marchisio *et al*., 1984; Pfaff and Jurdic, 2001; Baldassarre *et al*., 2006) containing proteins involved in actin nucleation such as Wiskott–Aldrich syndrome protein (WASP) (Linder *et al*., 1999; Mizutani *et al*., 2002) and Arp2/3 and cortactin (Bowden *et al*., 1999; Linder *et al*., 2000; Pfaff and Jurdic, 2001; Artym *et al*., 2006; Bowden *et al*., 2006; Luxenburg *et al*., 2006; Tehrani *et al*., 2006; Webb *et al*., 2007). The second part is a multimolecular complex surrounding the core and composed of integrin receptors and integrin-associated proteins also found in focal adhesions such as vinculin and talin (Linder and Aepfelbacher, 2003) or paxillin (Bowden *et al*., 1999; Pfaff and Jurdic, 2001). Paxillin is an adaptor protein initially found at cell extracellular matrix contacts in focal adhesions (Turner *et al*., 1990). It is highly phosphorylated on tyrosyl residues (Turner *et al*., 1990; Schaller, 2001), and it has been shown to regulate focal adhesion dynamics and cell migration (Nakamura *et al*., 2000; Petit *et al*., 2000; Brown and Turner, 2004; Vindis *et al*., 2004; Webb *et al*., 2004). The tyrosines 31 (Y31) and 118 (Y118) are preferential sites for

This article was published online ahead of print in *MBC in Press* (http://www.molbiolcell.org/cgi/doi/10.1091/mbc.E06–01–0088) on November 28, 2007.

Address correspondence to: Marc R. Block (marc.block@ujf-grenoble.fr).

phosphorylation inducing focal adhesion turnover and cell migration possibly through the binding of Crk (Birge *et al.*, 1993; Salgia *et al.*, 1995; Schaller and Parsons, 1995; Nakamura *et al.*, 2000; Petit *et al.*, 2000; Zaidel-Bar *et al.*, 2007).

Podosome/invadopodia dynamics and functions were reported to be regulated by the Rho family GTPases (Chellaiah *et al.*, 2000; Moreau *et al.*, 2003; Destaing *et al.*, 2005; Yamaguchi *et al.*, 2005; Gimona and Buccione, 2006), dynamin (Lee and De Camilli, 2002), and by Src-induced tyrosine phosphorylations (Marchisio *et al.*, 1984; Tarone *et al.*, 1985; Mueller *et al.*, 1992; Linder and Aepfelbacher, 2003; Bowden *et al.*, 2006). More specifically, c-Src was identified as a key regulator of osteoclast-mediated bone resorption (Yoneda *et al.*, 1993; Hall *et al.*, 1994).

Here, we described that Rous sarcoma virus (RSV)-transformed baby hamster kidney (BHK) cells have the ability to form successively invadopodia clusters, rings, and belt-like structures under the control of tyrosine phosphorylations. During these processes, invadopodia underwent a spatiotemporal organization that influenced their contact with the ECM. Paxillin phosphorylation on tyrosine 31 and 118 specifically stimulates invadopodia disassembly at the inner rim of the ring. The role of paxillin in controlling invadopodia ring dynamics was extended to the organization of osteoclast podosomes into rings and belts. The lack of paxillin phosphorylation, calpain or extracellular signal-regulated kinase (Erk) inhibition, resulted in similar phenotype, suggesting that these proteins belong to the same regulatory pathways. Indeed, paxillin phosphorylation promotes Erk activation that in turn was reported to activate calpain. Finally, we have shown that invadopodia/podosomes ring expansion is required for efficient extracellular matrix degradation both in BHK-RSV cells and primary osteoclasts, and for transmigration through a cell monolayer.

MATERIALS AND METHODS

Antibodies and Reagents

The following antibodies were used: monoclonal anti-paxillin (clone 349; BD Biosciences, Le Pont de Claix, France), polyclonal anti-phospho-Tyr31-paxillin and anti-phospho-Tyr118-paxillin (Biosource Europe, Nivelles, Belgium), monoclonal anti-cortactin (clone4F-11; Upstate Biotechnology, Charlottesville, VA), anti-β_3 integrin EDL1 (generously given by Dr. B. Nieswandt, Wuerzburg, Germany), monoclonal anti-phospho-tyrosine (clone 4G10; Upstate Biotechnology), monoclonal anti-vinculin (Millipore/Chemicon, St.-Quentin-Yvelines, France; AbCys, Paris, France) monoclonal anti-P-Erk (T202, Y204; Santa Cruz Biotechnology, Heidelberg, Germany), and polyconal anti-Erk 1/2 (New England Biolabs, Ipswich, MA; Ozyme, St.-Quentin-en-Yvelines, France). Horseradish peroxidase (HRP)-conjugated goat anti-mouse or goat anti-rabbit immunoglobulin (Ig)G were from Bio-Rad (Marnes-la-Coquette, France) and Jackson ImmunoResearch Laboratories (Soham, United Kingdom), respectively. Secondary antibodies Alexa-488– or Alexa-546–conjugated goat anti-mouse or goat anti-rabbit IgG were purchased from Invitrogen (Cergy Pontoise, France). Fluorescein isothiocyanate- (FITC) and tetramethylrhodamine B isothiocyanate (TRITC)-conjugated phalloidin were from Sigma (l'Isle d'Abeau, France). Sodium orthovanadate was from LC Laboratories (Woburn, MA), and it was prepared as a 100 mM stock solution in water. The calpain inhibitor was from Calbiochem (VWR International, Strasbourg, France), and it was prepared as a 24 mM stock solution in dimethyl sulfoxide (DMSO) and used at the final concentration 50 μM. The mitogen-activated protein kinase kinase (MEK)/Erk inhibitor U0126 was from Promega (Madison, WI), and it was prepared as a 10 mM stock solution in DMSO and used at the final concentration 100 μM.

cDNA Constructs

Human wild-type (WT) and Y31F/Y118F (YF) paxillin cDNAs were subcloned from pBabe vectors generously provided by Dr. M. Hiraishi (Department of Molecular Biology, Osaka Bioscience Institute, Suita, Osaka), into pEGFP-C1 (BD Biosciences) by using EcoR1 and BspE1 restriction enzymes and T4 DNA ligase. Vectors encoding pEGFP-cortactin and pDsRed-N1-cortactin were from Dr. P. Jurdic (Ecole Normale Supérieure, Lyon, France) (Destaing *et al.*, 2003).

Cell Culture and Transfection

Baby hamster kidney cells transformed by Rous sarcoma virus (BHK-RSV cells) were maintained in DMEM containing 10% fetal bovine serum, 100 U/ml penicillin, and 100 μg/ml streptomycin in a humidified air, 5% CO_2 atmosphere. For transient transfections, BHK-RSV cells were plated in 24-well plates 24 h before Exgen 500-mediated DNA transfer (Euromedex, Souffelweyersheim, France), according to the manufacturer's instructions, by using a total of 2 μg of DNA plasmid per well. For live cell imaging (videomicroscopy or fluorescence recovery after photobleaching experiments), cells were harvested 24 h after transfection by using a trypsin/EDTA solution and plated on Lab-Tek chambers (Nalgen; Nalge Nunc International, Rochester, NY) in a 37°C incubator under a 5% CO_2 atmosphere. Cells were imaged 24 h later at room temperature, in DMEM medium supplemented with 10% fetal calf serum (FCS) and 10 mM HEPES. For conventional immunofluorescence, cells were processed 48 h after transfection.

Knockdown of Paxillin in Primary Osteoclasts

Mouse differentiated osteoclasts from spleen were transfected twice with duplex of oligonucleotides targeting paxillin mRNA, in presence of Oligofectamine reagent (Invitrogen). Two RNA duplexes were used: (sense 5′-GAG-CCC-UCA-CCU-ACC-GUC-AU-TT-3′ and antisense 5′-AU-GAC-GGU-AGG-UGA-GGG-CUC-TT-3′ or alternatively, sense 5′-GUG-UGG-AGC-CUU-CUU-UGG-U-TT-3′ and antisense 5′-A-CCA-AAG-AAG-GCU-CCA-CAC-TT-3′). The two sequences targeted at paxillin mRNA did not overlap. For transfection, 50 μl of small interfering RNA (siRNA) at 20 μM was added to 250 μl of Opti-MEM (Invitrogen) and 50 μl of Oligofectamine to 250 μl of Opti-MEM. Both solutions were mixed and incubated 20 min at room temperature, and then they were added to the cells. After transfection, the cells were fixed with 3% phosphate-buffered saline (PBS)-paraformaldehyde (PFA), permeabilized in 0.1% PBS-Triton, and incubated with phalloidin-FITC for 1 h at 37°C for actin staining. Efficiency of siRNA-mediated paxillin silencing was checked by Western blotting and immunofluorescence analysis.

Immunofluorescence Microscopy

Cells grown on glass coverslips were fixed with 2.5% paraformaldehyde and 5% sucrose in PBS for 10 min at room temperature (RT), and then they were permeabilized in 0.1% Triton X-100 in PBS for 5 min. Coverslips were washed twice with PBS, blocked in 1% bovine serum albumin (BSA) in PBS and incubated for 1 h at RT with primary antibodies. Cells were rinsed in PBS, and secondary antibodies and TRITC-phalloidin were added for 1 h at RT. Coverslips were permanently mounted in Mowiol from Calbiochem (VWR International, Strasbourg, France) containing 4′6-diamidino-2-phenylindole. Fixed cells were examined using a confocal laser-scanning microscope (LSM 510; Carl Zeiss, Le Pecq, France), equipped with a 40× Plan Neo Fluor oil-immersion objective. For Scan Z analyses, successive planes in three-dimensional (3D) image stacks were taken every 0.1 μm. Images of interference reflection microscopy were obtained using the same objective equipped with the Wollaston prism and a 633-nm HeNe laser. The polarized light reflection was detected in channel 1 of a confocal microscope (LSM 510) equipped with polarization analyzer.

Videomicroscopy

Living BHK-RSV cells were imaged at room temperature by using the inverted confocal laser-scanning microscope with a 40×/numerical aperture (NA) 1.2 C-Apochromat water immersion objective. Cells were plated on Lab-Tek chambered glass slides in DMEM containing 10% FCS and 10 mM HEPES buffer. The pinhole was adjusted to 1.45 Airy unit. The green fluorescent protein (GFP) fluorescence was selected with NFT490 dichroic beamsplitter and BP500–550 band-pass filter; DsRed was detected using NFT543 dichroic beam-splitter and LP560 long-pass filter.

The fluorescence images were sampled with LSM510 3.2 software (Carl Zeiss, Jena, Germany) with a time lapse of 3, 5, or 7 min for a total recording of 99, 130, or 189 min, respectively, depending on the movie. The laser intensity on the sample was very low (750 μW with 3% acousto-optic tunable filter transmission), and no pronounced photobleaching or photothermal effects on cells were observed during the acquisition.

Each frame, in time-lapse movies, was processed for 2D-deconvolution by using No-neighbor algorithm of MetaMorph 6.0 (Molecular Devices, Sunnyvale, CA). Image comparison before and after deconvolution indicated that the restoration process did not generate any artifacts. Singular invadopodia movements were tracked using Object Tracking module of MetaMorph 6.0. Lifetimes of invadopodia were determined by measuring the time interval between the first appearance and complete disappearance of single invadopodia on the deconvoluted time-lapse movies.

Total Internal Reflection Fluorescence Microscopy (TIRF)

BHK-RSV cells were transiently transfected with paxillin-GFP and cortactin-DsRed, plated for 24 h on Lab-Tek chambered glass slides in DMEM containing 10% FCS and 10 mM HEPES buffer, treated with 5 mM orthovanadate for 30 min, and then observed with a TIRF microscope (Carl Zeiss). Cells were

imaged at 37°C every 3 min with both TIRF and epifluorescence. Images were extracted from stacks and treated with Adobe Photoshop (Adobe Systems, Mountain View, CA) for artificial colors attribution. Then, quantification of signals intensity along the ring was made using Volocity 2.6.3 Software (Improvision, Coventry, United Kingdom).

Western Blotting

Whole cell lysates were prepared in 50 mM Tris-HCl, pH 7.3, 75 mM NaCl, 1% Triton X-100, 0.1% SDS, 50 mM NaF, 40 mM sodium pyrophosphate, 1 mM orthovanadate (Na_3VO_4), 1 mM EDTA, 1 mM phenylmethylsulfonyl fluoride (PMSF), and 0.02% (vol/vol) protease inhibitor cocktail (complete EDTA-free; Roche Diagnostics, Mannheim, Germany). Then, 20 μg of proteins from each cell lysate was submitted to SDS-polyacrylamide gel electrophoresis (PAGE), transferred to nitrocellulose membranes, and probed with primary antibodies. HRP-conjugated goat anti-mouse or goat anti-rabbit secondary antibodies (from Bio-Rad, Hercules, CA, and Jackson ImmunoResearch Laboratories, West Grove, PA, respectively) were detected by enhanced chemiluminescence (GE Healthcare Europe, Saclay, France). Equal loading was assessed by protein staining on nitrocellulose membrane with Ponceau S (Sigma).

Coimmunoprecipitation

Whole cell lysates were prepared in 50 mM Tris-HCl, pH 7.3, 75 mM NaCl, 50 mM NaF, 40 mM sodium pyrophosphate, 1 mM Na_3VO_4, 1 mM EDTA, 1 mM PMSF, and 0.02% (vol/vol) protease inhibitor cocktail (complete EDTA-free; Roche Diagnostics). After a first incubation with 3% PBS-BSA for 1 h at 4°C, protein A-Sepharose beads (GE Healthcare) were then incubated with either an IgG 2A nonspecific antibody (Immunotech, Marseille, France) or with paxillin monoclonal antibody (mAb) for 2 h at 4°C. Then, 1 mg of total lysate was successively incubated with IgG 2A-coated beads and paxillin antibody-coated beads (overnight at 4°C). After centrifugation, the pellets were submitted to SDS-PAGE electrophoresis and Western blotting.

Extracellular Matrix Degradation Assays

The extracellular matrix was carried out by coating coverslips with TRITC-labeled gelatin diluted at 10 μg/ml in DMEM, for 24 h at 4°C. Then, the gelatin-TRITC–coated coverslips were fixed in 3% paraformaldehyde, 5% sucrose in PBS for 10 min at room temperature. After two washes with sterile PBS, the coverslips were coated with human vitronectin (BioSource International, Camarillo, CA) at 5 μg/ml in DMEM for 24 h at 4°C. Then, the coverslips were fixed and washed twice with sterile PBS. Finally, BHK-RSV cells or BHK-RSV cells transfected with paxillin-GFP were plated onto the coated coverslips in DMEM containing 10% FCS. After 24 h of culture, cells were fixed and observed with an inverted confocal laser-scanning microscope (LSM 510) equipped with a 40× numerical aperture (NA) 1.4 Plan Neo Fluor oil immersion objective Degradation of the extracellular matrix was evaluated by visualizing dark holes in the red matrix. Quantification of the degradation ability was established by calculating the relative degradation index: $D_R = 100 - [(I_A \times 100)/I_C)]$, with I_A representing intensity of the signal in the area of degradation and I_c representing intensity of the signal in control area without degradation.

Transmigration Assays

HeLa cells (0.4×10^6) were plated onto chambered Lab-Tek glass slides in DMEM containing 10% FCS, and then they were allowed to form a confluent monolayer over 24 h. Paxillin-GFP–transfected BHK-RSV cells were then seeded on top of the HeLa cell monolayer. After 24 h, all the cells were fixed and permeabilized in 0.1% Triton X-100 in PBS for 5 min and then stained with phalloidin-TRITC for 30 min. Cells were then washed twice with PBS and kept in PBS until observation under the microscope. BHK-RSV cells transmigration through the HeLa cell layer was observed by realizing Z scan analyses (successive planes in 3D image stacks were taken every 0.4 μm) by using an inverted confocal laser-scanning microscope (LSM 510) equipped with a 40×/NA 1.2-Apochromat water immersion objective.

4D Time Lapse Videomicroscopy

HeLa cells (0.4×10^6) were plated onto chambered Lab-Tek glass slides in DMEM containing 10% FCS, and then they were allowed to form a confluent monolayer over 24 h. Paxillin-GFP–transfected BHK-RSV cells were then seeded on top of the HeLa cell monolayer. After 24 h, the BHK-RSV transmigration through the HeLa cell layer was observed performing Z scan analyses (successive planes in 3D image stacks were taken every 0.4 μm) with a confocal laser-scanning microscope (LSM 510) equipped with a 40×/NA 1.2 C-Apochromat water immersion objective.

RESULTS

Invadopodia in BHK-RSV Cells Reorganize Sequentially into Clusters, Rings, and Belt-like Structures

In BHK-RSV cells plated onto glass coverslips, invadopodia core staining by an anti-cortactin mAb revealed that individual invadopodia could self-assemble into various patterns. These structures evolved over time: 24 h after plating, invadopodia were mostly organized into clusters and small rings sometimes incompletely formed or displaying irregular shapes with diameters <10 μm (Figure 1, A and C). Within 48 h, >50% of invadopodia rings had increased in diameter (>10 μm). At this stage, invadopodia were found in large circular-shaped rings and belt-like structures (Figure 1A). These observations suggested that invadopodia clusters and small rings self-organize during the early stages of cell attachment and maturate into larger rings and belt-like structures later, a process that has been described in differentiated osteoclasts (Destaing *et al*., 2003).

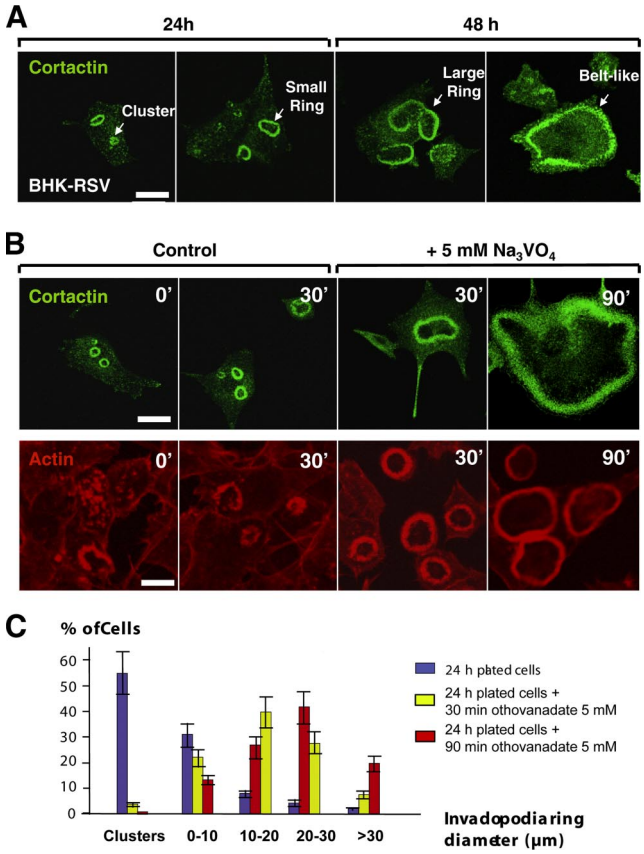

Figure 1. Dynamics of invadopodia in src-transformed BHK cells. (A) BHK-RSV cells were plated on glass coverslips for 24 or 48 h at 37°C, and then they were immunostained with an anti-cortactin mAb. Bar, 20 μm. (B) BHK-RSV cells plated for 24 h (control; 0 min) were treated either with the orthovanadate vehicle (H_2O) (control; 30 min) or with 5 mM orthovanadate for 30 min (+Na_3VO_4; 30 min) or 90 min (+Na_3VO_4; 90 min) before immunostaining for cortactin or actin. Bar, 20 μm. (C) Size distribution of invadopodia rings in BHK-RSV cells plated for 24 h without orthovanadate (blue line) and 24-h–plated cells and treated with 5 mM orthovanadate during 30 min (yellow line) or 90 min (red line), respectively (n = 60 cells for each condition).

Dynamic of Invadopodia Is Regulated by Tyrosine Phosphorylations

Invadopodia are very active sites of phosphorylation on tyrosyl residues (Marchisio *et al*., 1984; Tarone *et al*., 1985; Gavazzi *et al*., 1989; Mueller *et al*., 1992; Bowden *et al*., 2006). To address the role of this posttranslational modification, we treated BHK-RSV cells with the general tyrosine phospha-

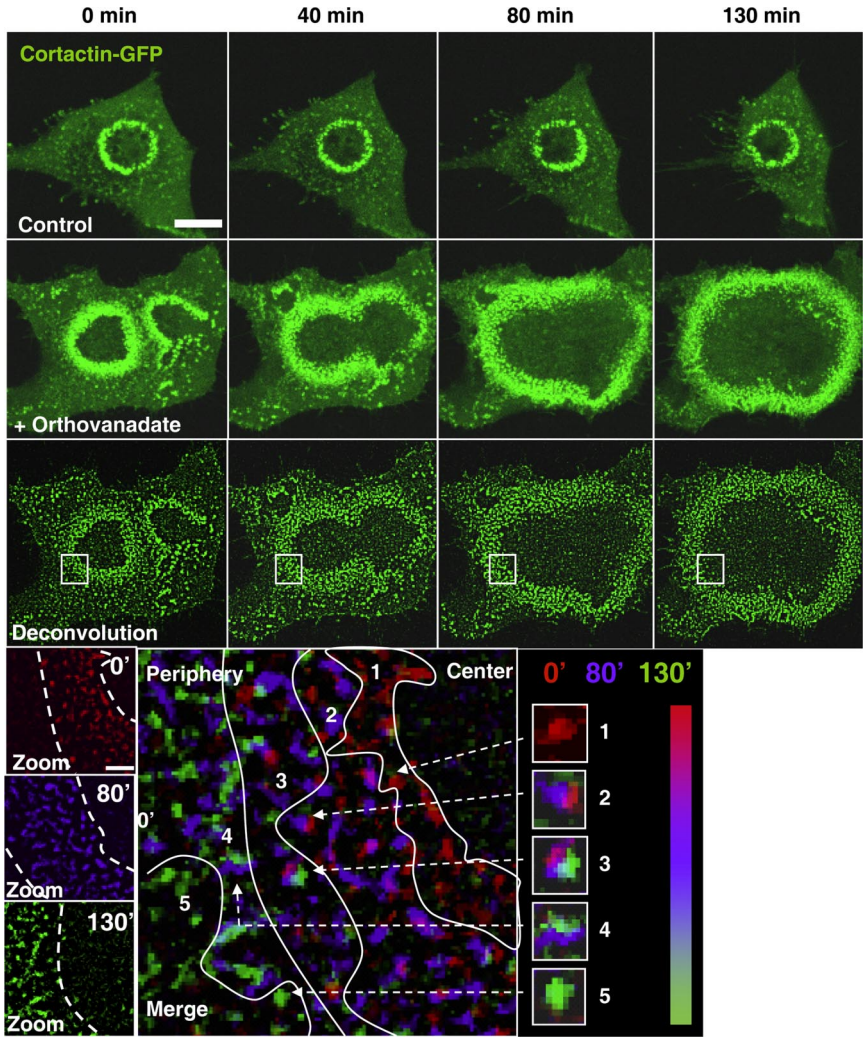

Figure 2. Orthovanadate-induced invadopodia ring expansion results from the coordinated processes of invadopodia assembly at the periphery and disassembly at the ring center. BHK-RSV cells plated for 24 h were transiently transfected with cDNA encoding cortactin-GFP. The expressed fusion protein was followed by time-lapse videomicroscopy for 130 min at room temperature, in the absence (control) or in the presence of 5 mM orthovanadate ($+Na_3VO_4$) by using a confocal microscope. Bar, 10 μm. Image deconvolution and zoom, using MetaMorph software revealed the individual invadopodia within the invadopodia rings. Merge of the images in false colors from 0 min (red), 80 min (blue), and 130 min (green) allowed following each invadopodia along the time course of the experiment. According to the color pattern, five regions could be defined from the center to the periphery of the ring that reflected both the spatiotemporal organization of invadopodia within the ring and the relative immobility of the individual invadopodia.

tase inhibitor Na_3VO_4 supplemented to the medium at the final concentration of 5 mM, after 24 h of preculture under standard conditions. Whereas untreated cells mainly displayed small rings whose diameter did not significantly increase within a subsequent 30-min period, orthovanadate addition induced, within 30 min, a dramatic increase in the size of invadopodia rings that was amplified together with the enhanced formation of belt-like structures at longer incubation times (Figure 1B). Quantification of these data is shown in Figure 1C. These results strongly suggest that the expansion of invadopodia rings is regulated by tyrosine phosphorylation events leading to the fast maturation of invadopodia rings into belt-like structures.

Tyrosine Phosphorylation Accelerates Invadopodia Turnover Resulting in Faster Ring Enlargement

To visualize the process of invadopodia ring enlargement, we performed time-lapse videomicroscopy analyses of BHK-RSV cells transfected with an invadopodia core protein, cortactin fused to GFP. In control cells, invadopodia rings displayed no diameter increase during the time course of the experiment (Figure 2 and Supplemental Movie 1), whereas during the same period in orthovanadate-treated cells invadopodia rings expanded and fused, leading to the formation of peripheral belt-like structures (Figure 2 and Supplemental Movie 2). Image deconvolution resolved the rings into individual invadopodia (Figure 2). The use of false colors and image merging at 0 min (red), 80 min (blue), and 130 min (green) allowed us to follow the spatiotemporal dynamics of each individual invadopodium (Figure 2, bottom). This representation clearly showed that although some slight tumbling was observed, invadopodia movements were inscribed within a small area (2.25 μm^2; n = 10), whereas at the same time the ring diameter increased from 10 μm to >30 μm. Peripheral invadopodia with the single red color at the ring center indicated that these structures were quickly disassembled at the beginning of the experiment. By contrast, at the ring periphery invadopodia showed up as a single green spot, indicating that they were newly formed.

At the intermediate position within the ring, each invadopodium displayed the three colors, indicating that these structures were always present during the time course of the experiment. These observations strongly suggested that the invadopodia ring enlargement was the result of coordinated processes of new invadopodia assembly at the ring periphery, whereas invadopodia located at the inner side disappeared without any sliding of these adhesive structures. Because the invadopodia ring width was approximately constant during expansion, tyrosine phosphorylation pro-

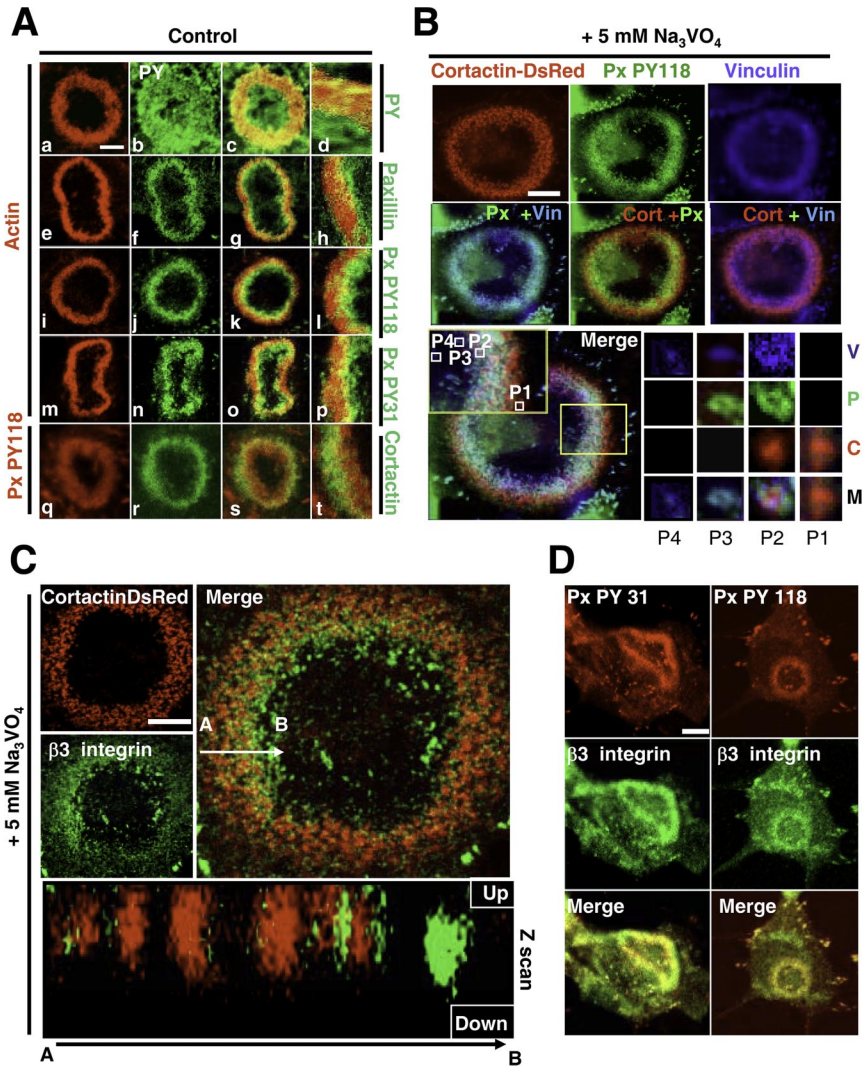

Figure 3. Endogenous paxillin is phosphorylated on tyrosine 31 and 118 and accumulates at the inner rim of the BHK-RSV invadopodia ring. (A) BHK-RSV cells were plated for 24 h on glass coverslips, and then they were stained for actin with phalloidin-TRITC (a) and the general phospho-tyrosine antibody 4G10 (b). Accumulation of tyrosine-phosphorylated proteins was observed at the ring center (merged images, c; zoom, d). Staining with a paxillin mAb revealed that endogenous paxillin (f) also accumulated at the center of the actin ring (e) (merge images g; zoom, h) together with phosphorylated paxillin on tyrosine 118 (PY118; j) and on tyrosine 31 (PY31; n) (i and m are actin staining). Changing the secondary antibody labeling did not modify the respective localization of paxillin (q) at the center of the ring and cortactin (r) at the periphery (merge images, s; zoom, t). Bar, 6 μm. (B) Cortactin-DsRed–transfected BHK-RSV cells were plated for 24 h on glass coverslips, and then they were treated with 5 mM Na_3VO_4 for 30 min. Invadopodia cores were specifically visualized by cortactin-DsRed (red). Endogenous phospho-paxillin and vinculin localizations were detected by specific monoclonal antibodies. Bar, 10 μm. Bottom, triple merged images. Zoom on four invadopodia (P1–P4) localized from the periphery (P1) to the ring center (P4) is presented. V, P, C, and M are vinculin, PY118 paxillin, cortactin-DsRed, and merge staining, respectively. Each invadopodia showed a specific composition. (C) BHK-RSV cells were transiently transfected with cortactin-DsRed, plated for 24 h, and treated subsequently with 5 mM Na_3VO_4 for 30 min before staining with a monoclonal anti-β_3 integrin antibody. Z scanning along the white arrow (A→B) reveals an increase in the length of invadopodia core along a cross section of the ring and β_3 integrins recruitment in invadopodia located at the inner rim of the ring. Bar, 10 μm. (D) BHK-RSV cells plated for 24 h were stained with anti-β_3 integrin antibody and phospho-specific polyclonal PY31 or PY118 paxillin antibodies. Bar, 10 μm.

moted by orthovanadate treatment favored both invadopodia assembly at the outer rim and dissociation at the inner rim of the ring, respectively. Consequently, these coordinated processes should result in the shortening of invadopodia lifetime. This was confirmed by direct measurement in orthovanadate-treated cells compared with untreated cells (59 ± 19 vs. 122 ± 13 min, respectively; n = 34; p = 0.014).

Phospho-paxillin Accumulates at Invadopodia Ring Center

Surprisingly, immunostaining of phospho-tyrosines in invadopodia ring of untreated BHK-RSV extended toward the ring center where actin was not detected by phalloidin-TRITC, and it was not present at the outer rim of the ring (Figure 3A, a–d). Because invadopodia were dissociated at the inner rim of the ring, this observation suggested that dismantling of invadopodia at the inner rim of the ring started with actin core disassembly at sites where a strong accumulation of tyrosyl-phosphorylated proteins occurred. Paxillin is a major target for tyrosine kinases, and it was reported to promote focal adhesion disassembly upon phosphorylation on tyrosines 31 and 118 (Brown and Turner, 2004; Zaidel-Bar *et al.*, 2007). Thereby, we hypothesized that paxillin, through its phosphorylation, could be responsible of invadopodia disassembly at the inner rim of the ring. Indeed, immunostaining of control BHK-RSV cells with a monoclonal anti-paxillin antibody (Figure 3A, e–h) or phospho-paxillin–specific antibodies (Figure 3A, i–p) revealed a similar localization than phospho-tyrosine staining, indicating that endogenous paxillin accumulated in a phosphorylated state on both tyrosine 118 and 31 at invadopodia ring centers. Inverting the green and red staining did not change the internal localization of phospho-paxillin, indicating that this pattern was not an optical artifact (Figure 3A, q–t).

Spatiotemporal Invadopodia Organization within Invadopodia Ring

Paxillin localization suggested a spatiotemporal change in invadopodia composition. Taking advantage of the accelerated ring dynamics induced by orthovanadate, we analyzed the invadopodia organization in BHK-RSV cells transiently transfected with the specific invadopodia core marker cortactin fused with DsRed. After a 30-min incubation with 5 mM orthovanadate to allow fast ring expansion, cells were fixed and immunostained with antibodies directed against vinculin and phospho-paxillin on tyrosine 118 (Figure 3B).

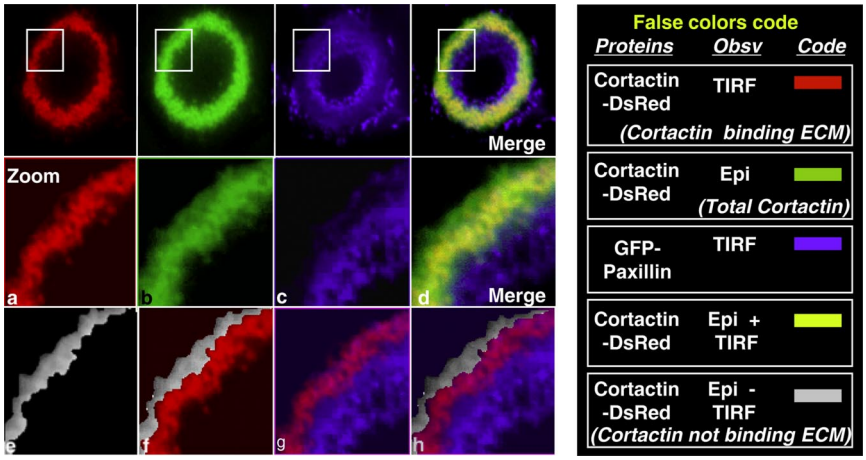

Figure 4. The inner rim of the invadopodia ring is a site of close contact with the extracellular matrix. BHK-RSV cells plated for 24 h were treated with 5 mM orthovanadate for 30 min and stained for GFP-paxillin and cortactin-DsRed. Fluorescence was visualized either by TIRF or by classical epi-illumination. For easier comparisons, the whole image was reconstituted with false colors. The ring displayed three regions from the periphery to the center: cortactin not in close contact with the matrix (gray), cortactin in contact with the matrix (red), and paxillin (blue) always in contact with the matrix.

Vinculin, phospho-paxillin, and talin (data not shown) accumulated at invadopodia located at the inner rim of the ring whereas the core protein cortactin was only present in invadopodia of the outer rim together with other core proteins such as actin, α-actinin, and dynamin (data not shown). These differential stainings clearly show a spatiotemporal change in invadopodia structure and composition: newly assembled invadopodia contained exclusively core proteins such as cortactin (Figure 3B, P1). Mature invadopodia were constituted by core proteins (cortactin), with surrounding proteins such as phospho-paxillin and vinculin (Figure 3B, P2). Finally, older invadopodia at the inner rim were devoid of any core protein (Figure 3B, P3), and eventually only vinculin was detected in the remaining structures (Figure 3B, P4).

The spatiotemporal organization of paxillin and cortactin was confirmed by time-lapse experiments performed on living BHK-RSV cells transiently transfected with both GFP-paxillin and cortactin-DsRed and then treated with 5 mM orthovanadate (Supplemental Figure S1 and Supplemental Movie 3). We observed that GFP-paxillin always maintained an internal localization compared with cortactin-DsRed and that it accumulated at sites where invadopodia cores progressively disappeared.

In podosome/invadopodia, paxillin is recruited indirectly by integrins (Gimona and Buccione, 2006). Immunofluorescence microscopy with anti-β_1 and anti-β_3 integrin antibodies in orthovanadate-treated BHK-RSV cells showed that β_1 integrins were excluded from invadopodia (data not shown), whereas β_3 integrin accumulated at invadopodia located at the inner rim of the ring (Figure 3C) where it was colocalized with phospho-paxillin (Figure 3D) suggesting that paxillin recruitment at the inner rim of the ring depends on integrins.

Differential ECM/Cell Contacts at Invadopodia Rings

Z Scan analysis showed that at the outer rim of the ring, invadopodia were mostly constituted of a cortactin core

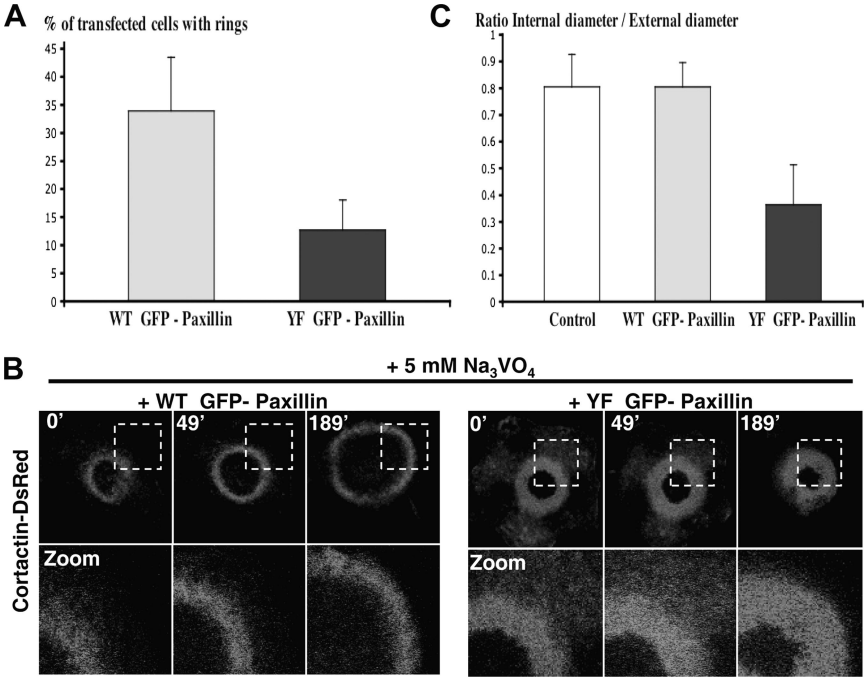

Figure 5. Mutant YF GFP-paxillin modifies invadopodia organization. (A) Decrease in the number of invadopodia rings of YF GFP-paxillin cells compared with WT GFP-paxillin cells under control conditions (n = 101 cells; p = 0.021). (B) BHK-RSV cells were double transfected with cortactin-DsRed and WT GFP-paxillin or YF GFP-paxillin, and treated or not with 5 mM orthovanadate as described previously. Evolution of invadopodia rings was followed by time-lapse videomicroscopy (only the red channel is shown). (C) Quantification of the relative thickness of the rings (internal diameter divided by external diameter) in the presence of orthovanadate, indicating a significant modification in invadopodia rings width (data from three independent experiments; n = 54; p value between control and WT = 0.5; p value between WT and YF, <0.001).

devoid of any β_3 integrins (Figure 3C). At a more central localization, invadopodia cores became longer and recruited β_3 integrins. Finally, at the inner rim of the rings, the cortactin core was no longer present, but the integrins remained. The increase in the core height during invadopodia maturation and the late recruitment of β_3 integrins suggests that invadopodia may not be in contact with the ECM during the early stages of core assembly at the ring periphery. This hypothesis was addressed by TIRF microscopy that allowed visualization of invadopodia components in proximity to the extracellular matrix. In this experiment, BHK-RSV cells were transiently transfected with both cortactin-DsRed and GFP-paxillin and treated with 5 mM orthovanadate. We compared images of cortactin-DsRed cores in contact with the matrix visualized by TIRF, with images of the whole Cortactin-DsRed cores obtained using classical epifluorescence (a similar analysis was carried out with GFP-paxillin). False colors were used to compare the over layered images (Figure 4). Cortactin stainings visualized by epifluorescence (green) and TIRF (red), respectively, did not fully match: epifluorescence signal extended beyond the periphery of the TIRF signal. This difference (colored gray) was interpreted as the amounts of nascent invadopodia at the ring periphery that had not yet reached the extracellular matrix. Conversely, no significant difference between GFP-paxillin epifluorescence, and TIRF signal was noticed indicating that all invadopodia containing paxillin were in contact with the support.

Lack of Paxillin Tyrosine Phosphorylation Impairs Invadopodia Disassembly at the Inner Rim of the Ring

Transient transfections of BHK-RSV cells with cDNAs encoding wild-type or mutant Y31F/Y118F GFP-paxillin named WT GFP-paxillin or YF GFP-paxillin, respectively, were carried out to address the role played by paxillin phosphorylation in invadopodia dynamics. Overexpression of paxillin mutants had a marked dominant-negative effect on the overall phosphorylation of paxillin within the cell, either in the presence (Figure 7C and Supplemental Figure S2) or absence (data not shown) of vanadate. The transfected cells were cultivated for 24 h on coverslips, and subsequently they were stained for actin with phalloidin-TRITC. Untreated cells expressing WT GFP-paxllin displayed normal invadopodia rings, whereas YF GFP-paxillin–expressing cells preferentially formed invadopodia clusters (Supplemental Figure S3). Statistical analyses (n = 101 cells; p =

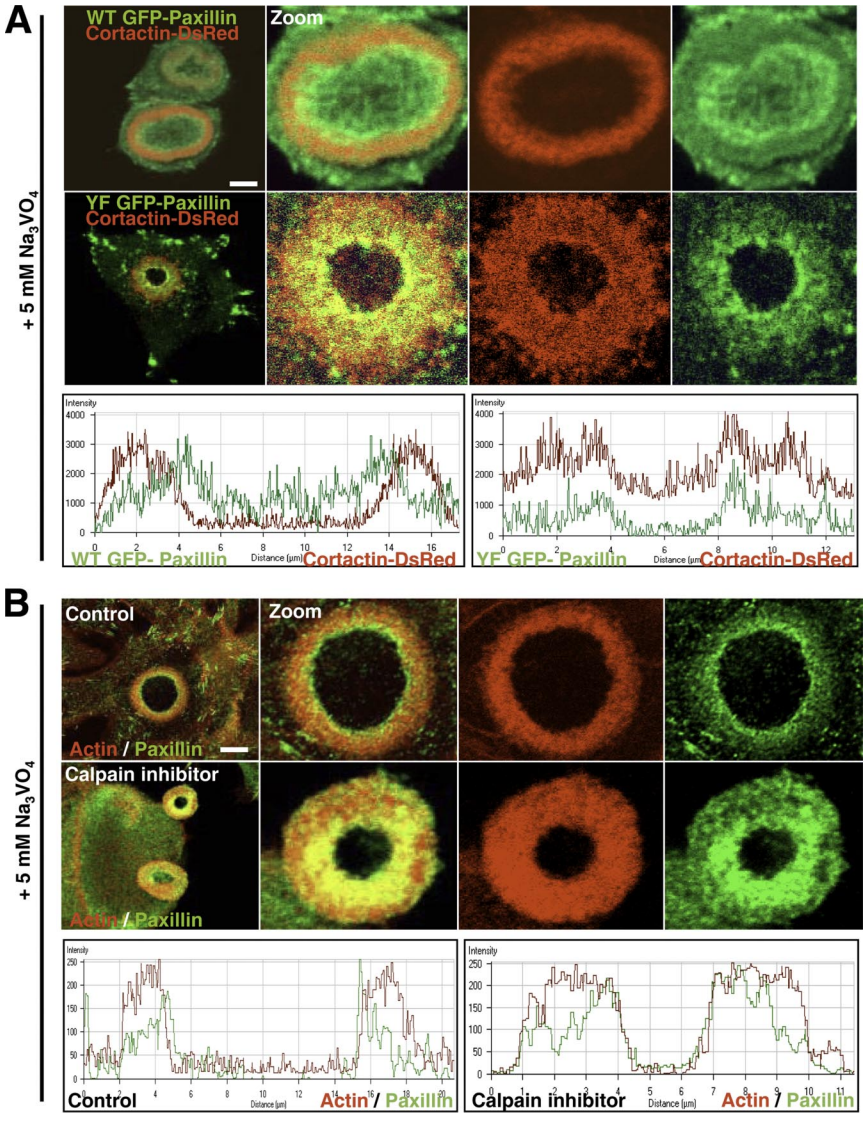

Figure 6. YF GFP-paxillin overexpression, or calpain inhibitor treatment, impairs invadopodia core disassembly. (A) BHK-RSV cells were double transfected with cortactin-DsRed and WT GFP-paxillin or YF GFP-paxillin and treated with 5 mM orthovanadate for 30 min. Then, cells were fixed with 3% paraformaldehyde. With WT GFP-paxillin cells, WT GFP-paxillin accumulated at the center of the rosette at sites where cortactin disassembled as shown on fluorescence intensity scans along the ring axis (bottom left). In YF GFP-paxillin cells, YF GFP-paxillin still accumulated at the center of the rosette, but cortactin did not dissociate at the rosette center, resulting in a much thicker ring and colocalization with YF GFP-paxillin (shown by fluorescence intensity scans along the ring axis; bottom right). (B) BHK-RSV cells treated with 50 μM ALLM calpain inhibitor and 5 mM orthovanadate for 30 min had thicker rings similar in structure and composition to those observed in YF GFP paxillin cells. Bar, 5 μm.

0.021) revealed that YF GFP-paxillin-transfected cells displayed fewer invadopodia rings than WT GFP-paxillin–transfected cells (Figure 5A). When ring expansion was accelerated by a 30-min treatment with 5 mM orthovanadate, the cells expressing WT GFP-paxillin exhibited invadopodia rings that were similar to those of untransfected cells. Under these experimental conditions, however, overexpression of YF GFP-paxillin induced the formation of much thicker rings with a reduced lumen (Figure 5B and Supplemental Figure S2). Statistical measurements of the ratio internal diameter/external diameter confirmed this observation (Figure 5C) (n = 54; p value between control and WT, 0.5; p value between WT and YF, <0.001). This result suggested that in presence of YF GFP-paxillin, new invadopodia cores formation at the ring periphery was not modified because the ring external diameter still increased, but invadopodia disassembly was somehow impaired at the ring center.

Blockade of Invadopodia Disassembly by Calpain Inhibition

WT GFP-paxillin accumulation at the ring center was always associated with the disappearance of cortactin-DsRed–rich cores (Figure 6A, left), whereas YF GFP-paxillin mutant clearly colocalized with cortactin-DsRed at the inner rim of the ring, confirming the defect in invadopodia disassembly (Figure 6A, right), suggesting that phosphorylation on paxillin is a prerequisite for invadopodia dissociation. Calpain is another protein that was reported to regulate podosomes disassembly (Calle *et al.*, 2006), possibly through cortactin proteolysis (Huang *et al.*, 1997). Therefore, we investigated whether in BHK-RSV cells, calpain inhibition could mimic the YF GFP-paxillin phenotype. We applied the calpain inhibitor ALLM at the final concentration 50 μM associated with 5 mM orthovanadate treatment for 30 min (to promote fast ring expansion). Actin staining clearly indicated that calpain inhibition was sufficient to inhibit invadopodia cores disassembly at the ring center and generated thick rings similar to what was observed under transfection of YF GFP-paxillin (Figure 6B, right). Moreover, under these experimental conditions, Western blotting revealed a marked decrease in cortactin degradation (data not shown). Together, these findings suggested that calpain is positioned downstream of paxillin phosphorylation in the invadopodia disassembly regulatory pathway.

Paxillin Phosphorylation on Tyrosine 31 and 118 Controls Erk Activation in Invadopodia Rings

The mitogen-activated protein kinases Erk1 and 2 are involved in the FAK/Src/paxillin signaling pathway driving focal adhesions disassembly (Webb *et al.*, 2004). Moreover, it has been reported that Erk can activate calpain (Glading *et al.*, 2001). Therefore, we hypothesized that paxillin could activate calpain through Erk signaling, resulting in invadopodia disruption. Indeed, coimmunoprecipitation experiments carried out with lysates from BHK-RSV cells revealed that paxillin and Erk interacted within a same molecular complex (Figure 7B). Moreover, immunofluorescence analysis showed that phospho-Erk (P-Erk) was present not only in the nucleus but also was enriched with phospho-paxillin into invadopodia rings (Figure 7A). Western blotting with P-Erk and Erk antibodies revealed that without orthovanadate, the levels of P-Erk were similar in WT GFP-paxillin and YF GFP-paxillin cells. Conversely, stimulating tyrosine phosphorylation by orthovanadate markedly increased the phosphorylation level of Erk in WT GFP-paxillin cells, but it had no significant effect on P-Erk levels in YF GFP-paxillin cells (Figure 7C). Indeed, overexpression of YF GFP-paxillin had a dominant-negative effect on endogenous paxillin phosphorylation that is reduced by at least 45% (Figure 7C and Supplemental Figure S3). Together, these results suggested that Erk phosphorylation and thereby its activation is regulated by paxillin phosphorylation on tyrosine 31 and 118 in invadopodia rings.

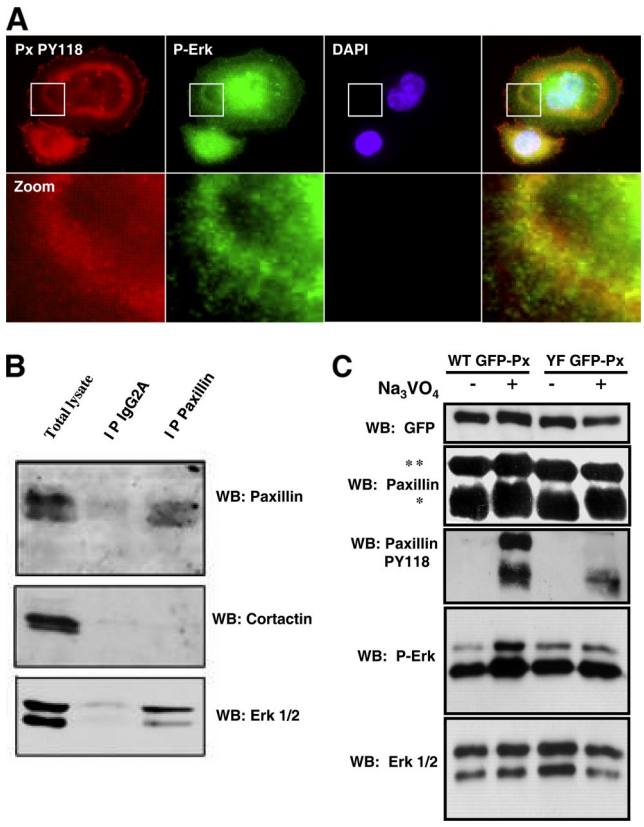

Figure 7. Orthovanadate-dependent Erk activation is controlled by paxillin phosphorylation on tyrosine 31 and 118. (A) In BHK-RSV cells, endogenous paxillin coimmunoprecipitates with Erk but not with cortactin. (B) In BHK-RSV cells, P-Erk is enriched invadopodia rings together with PY118 paxillin. (C) Western blotting carried out with lysates from polyclonal population of cell lines expressing WT GFP-paxillin (WT GFP-Px) or YF GFP-paxillin (YF GFP-Px), respectively, and treated or not with 5 mM orthovanadate for 30 min. *, endogenous paxillin; **, GFP paxillin. Equal protein loadings were assessed by proteins staining with Red Ponceau S (data not shown).

Erk Activation Is Required for Invadopodia Disassembly in Invadopodia Rings

To address to possible role of Erk phosphorylation in invadopodia core disassembly, we treated BHK-RSV cells with U0126 (a specific noncompetitive inhibitor of Erk kinase activity; Favata *et al.*, 1998) at the final concentration of 100 μM. Then, we measured the thickness of the rings after 30-min treatment with orthovanadate. Invadopodia core immunostaining with anti-cortactin revealed that U0126 induced invadopodia rosette thickening similarly to what was observed upon expression of YF GFP-paxillin, or calpain inhibition, suggesting that Erk inhibition prevented invadopodia cores disassembly at the inner rim of the ring (Figure 8, A and B). The similarities in the phenotypes suggested that Erk activation was acting upstream of calpain. This hypothesis was confirmed by intracellular calpain activity measurements indicating that calpain activity was

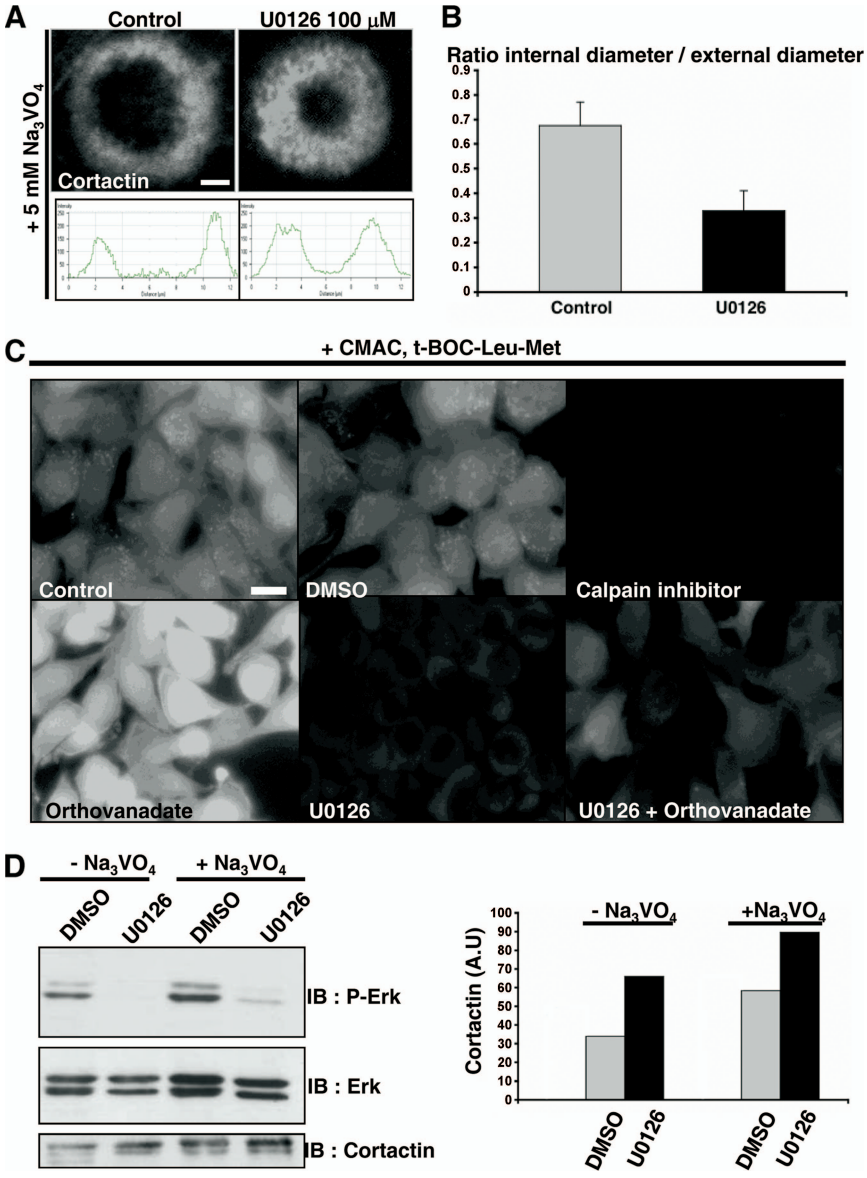

Figure 8. Inhibition of Erk phosphorylation by U0126 prevents invadopodia cores disassembly. (A) BHK-RSV cells were treated with 100 μM Erk inhibitor U0126. They formed thick invadopodia rings under orthovanadate treatment (5 mM; 30 min). Bar, 2 μm. (B) Statistical measures of invadopodia rings thickness in cells treated or not with U0126 after orthovanadate treatment. (C) BHK-RSV cells were treated with either DMSO or calpain inhibitor ALLM at 50 μM (1 h), orthovanadate at 5 mM (30 min), UO126 at 100 μM (1 h), UO126 at 100 μM (1 h), and then orthovanadate at 5 mM (30 min). After each treatment, cells were supplemented with CMAC t-Boc-Leu-Met (Invitrogen) at 50 μM (10 min) and fixed with 3% PBS-PFA. Cells were mounted and analyzed by fluorescence microscopy. Bar, 10 μm. (D) Western blotting showing that Erk inhibitor U0126 increased cortactin level either with or without orthovanadate treatment. Equal protein loading was checked by proteins staining on the nitrocellulose membrane with Red Ponceau S (data not shown).

mostly wiped out by blocking Erk with U0126 (Figure 8C) and by Western blotting showing that Erk inhibition by U0126 induced a reduction in cortactin degradation (Figure 8D). Together, our results strongly suggested that Erk activation is responsible of calpain-driven disassembly of invadopodia with the rings.

Generalization of Paxillin Role Invadopodia and Podosome Dynamics

The role of paxillin in podosome/invadopodia dynamics in a more physiological context was tested in primary mature osteoclasts in culture that exhibited podosomes organized into a classical peripheral belt. Similarly to invadopodia ring of BHK-RSV cells, paxillin accumulated at the inner rim of the podosome belt (Figure 9A). The same distribution was observed using phospho-paxillin–specific antibodies (data not shown). This suggested that paxillin could be also involved in osteoclast podosomes dynamics. We knocked down paxillin using siRNA in differentiated mouse primary osteoclasts. The efficiency of the knockdown was checked by Western blotting (Figure 9B). After paxillin knockdown, podosomes were no longer self-organized into a belt, but rather they remained as a cluster of podosomes (Figure 9C). We concluded that paxillin was also required for organization of podosome rings in this physiological model.

Lack of Invadopodia Ring Organization Impairs Extracellular Matrix Degradation

We investigated the possible effects of Y31F/Y118F paxillin mutations on invadopodia functions, such as extracellular matrix degradation. We observed that 24-h plated BHK-RSV cells could efficiently degrade an extracellular matrix constituted by one layer of gelatin-TRITC covered by one layer of vitronectin (a ligand of $\alpha_v\beta_3$ integrins) at invadopodia ring sites. Fully degraded matrix showed up as a dark trail left behind the invadopodia actin rings, probably due to the migration of the cell that displaced the ring underneath degradation took place (Figure 10A, control). It is noteworthy that differentiated primary mouse osteoclasts exhibiting podosomes could similarly degrade this organic matrix

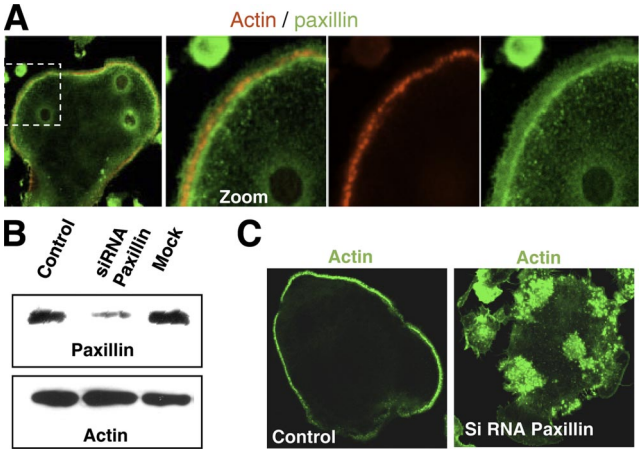

Figure 9. Paxillin knockdown impairs podosomes organization in primary mature osteoclasts. (A) Differential localization of actin and paxillin in the podosome belt of primary differentiated mouse osteoclasts on coverslips. The cells were fixed with 3% paraformaldehyde and stained for actin with phalloidin-TRITC and anti-paxillin antibodies. (B) siRNA paxillin performed in differentiated primary mouse osteoclasts. Western blot analysis showing the silencing of the protein paxillin (siRNA paxillin), compared with control cell treated with Oligofectamine alone (mock). (C) Differential organization of podosomes upon paxillin knockdown.

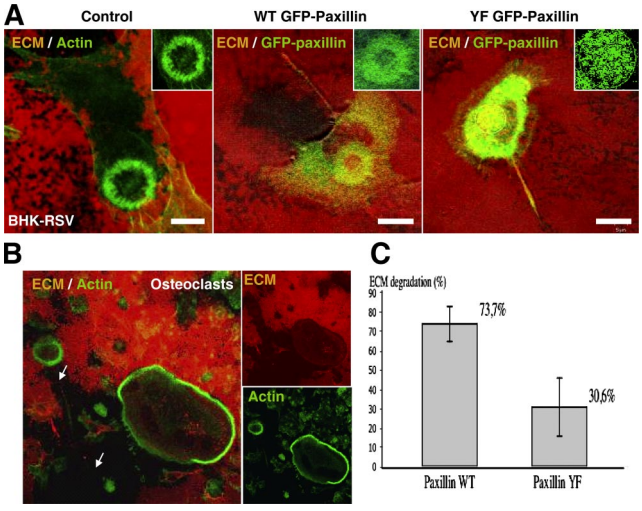

Figure 10. Extracellular matrix degradation takes place at the invadopodia/podosomes ring and is reduced by YF GFP paxillin overexpression. (A) Transfected and control BHK-RSV cells were plated 24 h on an extracellular matrix constituted by a layer of gelatin-TRITC fixed with 3% paraformaldehyde and covered by a layer of vitronectin. Left and middle, efficient matrix degradation by the control and WT GFP paxillin cells, respectively, at the level of the invadopodia rings. Right, BHK-RSV cells transfected with YF GFP-paxillin plated 24 h on the gelatin TRITC/vitronectin matrix. The ECM exhibited small and sparse patches of proteolysis corresponding to the individual disorganized invadopodia. Bar, 10 μm. (B) Differentiated primary mouse osteoclasts were plated on the gelatin-TRITC/vitronectin matrix for 24 h, fixed with 3% paraformaldehyde, and stained for actin with phalloidin-FITC. Degradation of this organic matrix is observed within the area defined by the podosome belt. (C) Quantification of the degradation ability of the extracellular matrix was established by calculating the relative degradation index D_R. (data from 3 independent experiments; n = 48 cells; $p < 0.001$).

without any need of mineralization (Figure 10B). Expression of WT GFP-paxillin did not impair matrix degradation (Figure 10A, GFP WT-paxillin). By contrast, expression of YF GFP-paxillin dramatically reduced extracellular matrix degradation. Although each invadopodia corresponded to a

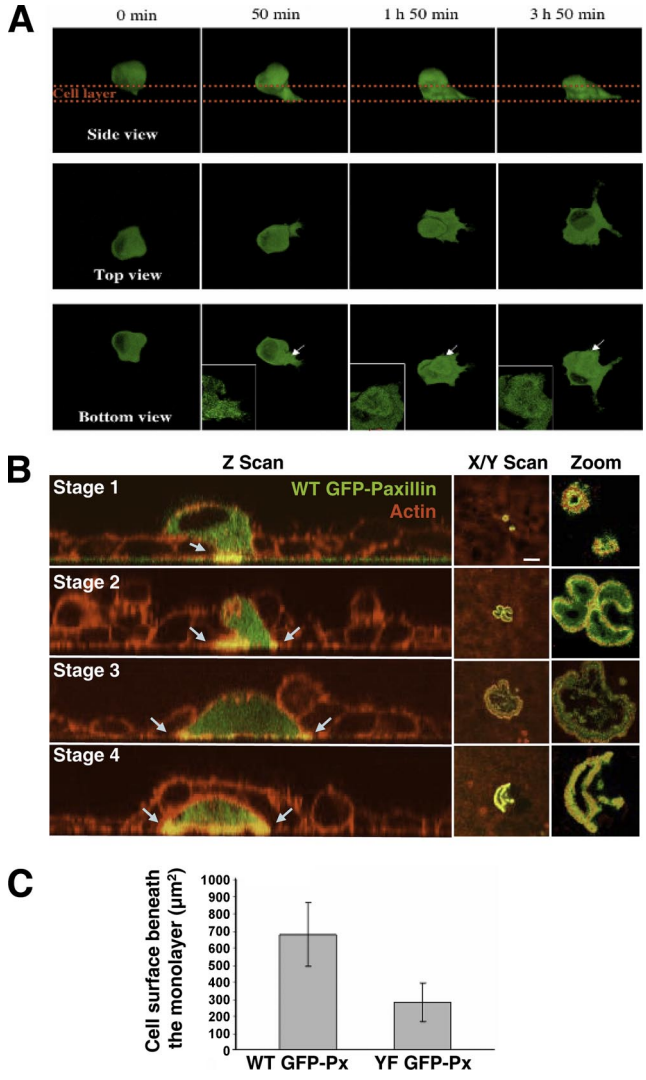

Figure 11. Invadopodia ring expansion promotes BHK-RSV cells transmigration through a cell monolayer. (A) 4D time-lapse videomicroscopy showing a single WT GFP-paxillin–transfected BHK-RSV cell crossing a HeLa cell monolayer (outlined by the red lines) and observed from side, top, and bottom views. The side view shows the sliding of the cell trough the cell layer, whereas the bottom view shows that in the same time at the ventral membrane, the cell formed an invadopodia ring that expanded toward the periphery of the area in contact with the matrix. (B) BHK-RSV cells transfected with WT GFP-paxillin were seeded on top of a HeLa cell monolayer in a Lab-Tek chamber. After 24 h, the cells were fixed in 3% paraformaldehyde, permeabilized with 0.1% Triton X-100 in PBS, stained for actin with TRITC-phalloidin, and observed by confocal microscopy (Z scan and X/Y scan). Stage 1, view of a BHK-RSV cell sending a membrane protrusion through the cell layer, ended by an invadopodia ring (yellow staining and arrows). Stage 2, a BHK-RSV cell crosses the cell layer. Z scan revealed an invadopodia ring (yellow staining and blue arrows) that slides under the neighboring cells. Stage 3, enlargement of the rosette pull down BHK-RSV cell under the HeLa monolayer. Stage 4, complete transmigration of a BHK-RSV cell through the cell monolayer. Bar, 10 μm. (C) Ovrexpression of YF GFP-paxillin in BHK-RSV cells diminished the average surface in contact with the matrix beneath the HeLa monolayer (n = 58; $p < 0.001$).

small area of degradation, these degradation spots remained disperse, probably due to the lack of invadopodia self-organization into rings, resulting in an overall lower efficiency in matrix proteolysis (Figure 10A, YF GFP-paxillin). The impaired matrix degradation was quantified by the relative degradation index described in *Materials and Methods*. Statistical measurements of the relative degradation index indicated that the expression of YF GFP-paxillin reduced by 2.4-fold the ability of cells to degrade the matrix compared with WT GFP-paxillin–transfected cells ($n = 48$ cells; $p < 0.001$) (Figure 10C).

Paxillin Y31F/Y118F Overexpression Alters Transmigration of BHK-RSV Cells through a Cell Monolayer

Matrix degradation and cell transmigration are often associated with invasiveness of cancer cells (Yamaguchi *et al*., 2005). To check the possible role of invadopodia dynamics in transmigration, BHK-RSV cells were transfected with WT GFP-paxillin and plated on a HeLa cells monolayer. After 24 h, time-lapse videomicroscopy in 4D (3 space dimensions + time) was carried out and allowed us to visualize cells crossing the layer along the time from different side, top, and bottom views (Figure 11A and Supplementary Movies 4, A–C). The progressive sliding of the BHK-RSV cell under the cell layer (Figure 11A, side view) was associated with the expansion of an invadopodia ring located at the ventral membrane of the cell (Figure 11A, bottom view), suggesting that invadopodia ring expansion could play a role in this process. Immunofluorescence experiments with BHK-RSV cells fixed after 24-h plating on the cell monolayer and stained for actin with phalloidin-TRITC were carried out. Observation of the cells by confocal microscopy along the *z*-axis allowed us to have a better insight of invadopodia ring formation during transmigration. At the early stages, BHK-RSV cells on the top side of the cell layer sent a membrane protrusion through the cell layer that reached the extracellular matrix. At this contact the membrane protrusion exhibited a small invadopodia ring (Figure 11B, stage 1). Subsequently, the cells displayed large invadopodia rings sliding under the neighboring cells of the layer (Figure 11B, stage 2). Later on, large well-formed invadopodia belt allowed the full spreading of the BHK-RSV cells beneath the cell layer (Figure 11B, stage 3), and finally, BHK-RSV cells were fully located on the bottom face of the cell monolayer (Figure 11B, stage 4).

According to these experiments, invadopodia dynamics seemed to be tightly related to transmigration. Because paxillin tyrosine phosphorylation could efficiently alters this process we investigated the role of paxillin phosphorylation in cell transmigration. We expressed YF GFP-paxillin into BHK-RSV cells. As expected, these cells presented markedly restricted spreading areas under the cell layer, compared with WT GFP-paxillin (Figure 11C; $n = 58$; $p < 0.001$) strongly suggesting that paxillin tyrosine phosphorylation through its involvement in invadopodia ring expansion favors the spreading of the transformed cells onto basal membrane that in turn triggered efficient transmigration through a cell layer.

DISCUSSION

Here, we describe that RSV-transformed BHK cells exhibit invadopodia that self-organize into large invadopodia rings and peripheral invadopodia belts, which are similar to podosomes found in macrophages and osteoclasts. These large structures were observed 48 h after plating the cells on glass; thus, they have much slower dynamics that podosomes in osteoclasts. However, orthovanadate, a general tyrosine phosphatase inhibitor, dramatically accelerates the process of invadopodia ring expansion into large rings and invadopodia belts. It is noteworthy that the time of preculture in serum supplemented media is likely sufficient to allow vitronectin and fibronectin coating on the glass slide. Previous studies carried out with RAW 264.7 cells differentiated into osteoclasts indicated that podosome ring expansion results from the assembly of new podosomes at the ring periphery together with podosome disassembly at inner rim of the ring (Destaing *et al*., 2003). These two processes are coordinated and maintain a relative constant ring width during expansion. Taking advantage of the acceleration of invadopodia ring expansion induced by orthovanadate in src-transformed BHK cells and using time-lapse videomicroscopy coupled with 2D deconvolution and object tracking, we demonstrated that invadopodia followed identical behavior in BHK-RSV cells. Because orthovanadate-treated invadopodia rings maintained a constant width during their expansion, tyrosine phosphorylations probably promote both new invadopodia formation at the ring periphery and invadopodia disassembly at the ring center: two mechanisms that account for the acceleration of the ring expansion. This view is consistent with the well-described action of Src-induced tyrosine phosphorylations that promote invadopodia assembly (Mueller *et al*., 1992; Bowden *et al*., 2006). Additionally, orthovanadate was shown to induce podosomes formation in monocytes and fibroblasts (Marchisio *et al*., 1988; Cory *et al*., 2002) confirming the importance of tyrosine phosphorylation in podosomes assembly.

Actin nucleating factors such as cortactin and WASP also seemed to play a major role in podosome assembly depending on their phosphorylation on tyrosine by Src (Linder and Aepfelbacher, 2003; Artym *et al*., 2006; Tehrani *et al*., 2006). Thus, it can be hypothesized that Src may promote a strong nucleation of actin polymerization at the locus of a new invadopodia formation. Additionally, optical flow analysis suggests that the initial organization into clusters and small rings may result from spontaneous self-organization of actin, whereas life span and distance between invadopodia/podosome depend on the substrate flexibility (Collin *et al*., 2006). By contrast, little is known on podosome/invadopodia disassembly. Interestingly, tyrosine phosphorylation has been described to promote focal adhesion turnover (Webb *et al*., 2004; Westhoff *et al*., 2004). More specifically, focal adhesion disassembly seems to be triggered by the phosphorylation of paxillin on tyrosine 31 and 118 (Brown and Turner, 2004; Zaidel-Bar *et al*., 2007). Because paxillin is also a major invadopodia/podosome component, it was tempting to make a parallel and to hypothesize that tyrosine-phosphorylation on paxillin is also involved in invadopodia core disassembly resulting in fine, in the complete dismantling of invadopodia. Consistent with this idea, we have shown that tyrosine 31/118 phosphorylated paxillin and β_3 integrins accumulated preferentially at the inner rim of the ring where invadopodia had a tight contact with the matrix and progressively loosed their actin rich core. Moreover, overexpression of a phosphorylation-deficient paxillin-GFP Y31F/Y118F mutant clearly impaired invadopodia actin core disassembly. On orthovanadate treatment that favored fast ring expansion, this mutation resulted in the thickening of invadopodia rings with small lumens due to the inability of inner invadopodia to dismantle.

TIRF and Scan Z confocal microscopy indicated that at the early stages of invadopodia assembly, the actin core was increasing in height toward the matrix. At this stage, the newly formed invadopodia were not in contact with the extracellular matrix. Once this actin core-driven membrane

protrusion had reached the extracellular matrix, β_3 integrin and integrin-associated proteins such as vinculin and paxillin were recruited and surrounded the actin core, giving rise to the classical invadopodia/podosome structure. Finally, paxillin phosphorylation seemed to be a prerequisite for core disassembly and eventually the complete disappearance of the structure. This spatiotemporal evolution is consistent with published data showing that invadopodia display different stages depending on the time contact with the extracellular matrix (Artym *et al*., 2006). These authors reported that during the last stage, invadopodia have lost their actin core, and in meantime massively recruited MT1-MMP promoting ECM degradation. Interestingly, we showed that podosomes in osteoclast cells could also induce the efficient degradation of the ECM, in vitro, although it has been commonly considered that these structures have a poor proteolytic activity.

Transfecting the cells with YF GFP-paxillin, by using the calpain inhibitor ALLM or U0126, a specific Erk inhibitor, resulted in similar alteration of invadopodia rings in the presence of orthovanadate, strongly suggesting that all these signaling molecules belong to the same signaling pathway. Within this pathway, paxillin phosphorylation is likely acting upstream because the YN GFP mutant impairs Erk activation. Crk is a good potential candidate for signaling downstream of paxillin in invadopodia because it was shown to control migration and invasion of transformed cells (Rodriguez and Guan, 2005). The adaptor protein Crk-associated substrate (Cas), which links Crk, was also described as essential for invasion and metastasis of src-transformed cells by activating the small GTPase Rac1 (Brabek *et al*., 2005). Thereby, tyrosine phosphorylation of paxillin could induce Crk/Cas recruitment and promote Erk activation through Rac1 activation. In turn, we have shown that Erk was required to activate calpain in good agreement with previous work (Glading *et al*., 2001).

Finally, our work shows that efficient matrix degradation by BHK-RSV cells requires invadopodia ring assembly. This probably results from local concentration of matrix proteases within the ring. Indeed, with YF GFP-paxillin mutant, when invadopodia mostly self-organize into clusters, the dot-like matrix degradation suggests that matrix protease delivery at invadopodia still occurs, but the invadopodia disorganization seemed to prevent massive matrix degradation. Invadopodia ring expansion seems to be also involved in transmigration of BHK-RSV cells through a cell layer. The invadopodia ring is known to be a site of strong anchorage of the cell on the matrix while invadopodia touch the extracellular matrix beneath the cell monolayer. Scan Z confocal microscopy suggests that ring expansion may allow spreading that trigger the mechanical force that pulls the cell body through the monolayer while providing a localized site of matrix degradation. Such behavior may be a general mechanism for invasion of metastatic cells. Because these processes are upstream controlled by paxillin phosphorylation, this protein seems to be a potential target for the design of anti-metastatic drugs.

ACKNOWLEDGMENTS

This article is dedicated to the memory of Martin Pfaff who enthusiastically initiated this project. We thank Dr. B. Nieswandt for providing anti-β_3 integrin mAb and Dr. Manami Hiraishi for the gift of pBabe-paxillin vectors. This work was supported by the Centre National de la Recherche Scientifique and by funding from the Région Rhône-Alpes (Programme Emergence) and by a grant from the Institut de la Longévité (GISLO401 Institut National de la Santé et de la Recherche Médicale) (to G.P.). C.B. was the recipient of a doctoral fellowship from the French Ministry of Research and Higher Education and the Association pour la Recherche contre le Cancer (ARC). ARC association is also acknowledged for the financial support of the imaging facilities.

REFERENCES

Abram, C. L., Seals, D. F., Pass, I., Salinsky, D., Maurer, L., Roth, T. M., and Courtneidge, S. A. (2003). The adaptor protein fish associates with members of the ADAMs family and localizes to podosomes of Src-transformed cells. J. Biol. Chem. *278*, 16844–16851.

Artym, V. V., Zhang, Y., Seillier-Moiseiwitsch, F., Yamada, K. M., and Mueller, S. C. (2006). Dynamic interactions of cortactin and membrane type 1 matrix metalloproteinase at invadopodia: defining the stages of invadopodia formation and function. Cancer Res. *66*, 3034–3043.

Ayala, I., Baldassarre, M., Caldieri, G., and Buccione, R. (2006). Invadopodia: a guided tour. Eur. J. Cell Biol. *85*, 159–164.

Baldassarre, M., Ayala, I., Beznoussenko, G., Giacchetti, G., Machesky, L. M., Luini, A., and Buccione, R. (2006). Actin dynamics at sites of extracellular matrix degradation. Eur. J. Cell Biol. *85*, 1217–1231.

Baldassarre, M., Pompeo, A., Beznoussenko, G., Castaldi, C., Cortellino, S., McNiven, M. A., Luini, A., and Buccione, R. (2003). Dynamin participates in focal extracellular matrix degradation by invasive cells. Mol. Biol. Cell *14*, 1074–1084.

Birge, R. B., Fajardo, J. E., Reichman, C., Shoelson, S. E., Songyang, Z., Cantley, L. C., and Hanafusa, H. (1993). Identification and characterization of a high-affinity interaction between v-Crk and tyrosine-phosphorylated paxillin in CT10-transformed fibroblasts. Mol. Cell. Biol. *13*, 4648–4656.

Bowden, E. T., Barth, M., Thomas, D., Glazer, R. I., and Mueller, S. C. (1999). An invasion-related complex of cortactin, paxillin and PKCmu associates with invadopodia at sites of extracellular matrix degradation. Oncogene *18*, 4440–4449.

Bowden, E. T., Onikoyi, E., Slack, R., Myoui, A., Yoneda, T., Yamada, K. M., and Mueller, S. C. (2006). Co-localization of cortactin and phosphotyrosine identifies active invadopodia in human breast cancer cells. Exp. Cell Res. *312*, 1240–1253.

Brabek, J., Constancio, S. S., Siesser, P. F., Shin, N. Y., Pozzi, A., and Hanks, S. K. (2005). Crk-associated substrate tyrosine phosphorylation sites are critical for invasion and metastasis of SRC-transformed cells. Mol. Cancer Res. *3*, 307–315.

Brown, M. C., and Turner, C. E. (2004). Paxillin: adapting to change. Physiol. Rev. *84*, 1315–1339.

Buccione, R., Orth, J. D., and McNiven, M. A. (2004). Foot and mouth: podosomes, invadopodia and circular dorsal ruffles. Nat. Rev. Mol. Cell Biol. *5*, 647–657.

Collin, O., Tracqui, P., Stephanou, A., Usson, Y., Clement-Lacroix, J., and Planus, E. (2006). Spatiotemporal dynamics of actin-rich adhesion microdomains: influence of substrate flexibility. J. Cell Sci. *119*, 1914–1925.

Calle, Y., Carragher, N. O., Thrasher, A. J., and Jones, G. E. (2006). Inhibition of calpain stabilises podosomes and impairs dendritic cell motility. J. Cell Sci. *119*, 2375–2385.

Chellaiah, M. A., Soga, N., Swanson, S., McAllister, S., Alvarez, U., Wang, D., Dowdy, S. F., and Hruska, K. A. (2000). Rho-A is critical for osteoclast podosome organization, motility, and bone resorption. J. Biol. Chem. *275*, 11993–12002.

Cory, G. O., Garg, R., Cramer, R., and Ridley, A. J. (2002). Phosphorylation of tyrosine 291 enhances the ability of WASp to stimulate actin polymerization and filopodium formation. Wiskott-Aldrich syndrome protein. J. Biol. Chem. *277*, 45115–45121.

Destaing, O., Saltel, F., Geminard, J. C., Jurdic, P., and Bard, F. (2003). Podosomes display actin turnover and dynamic self-organization in osteoclasts expressing actin-green fluorescent protein. Mol. Biol. Cell *14*, 407–416.

Destaing, O., Saltel, F., Gilquin, B., Chabadel, A., Khochbin, S., Ory, S., and Jurdic, P. (2005). A novel Rho-mDia2-HDAC6 pathway controls podosome patterning through microtubule acetylation in osteoclasts. J. Cell Sci. *118*, 2901–2911.

Favata, M. F. *et al*. (1998). Identification of a novel inhibitor of mitogen-activated protein kinase kinase. J. Biol. Chem. *273*, 18623–18632.

Gavazzi, I., Nermut, M. V., and Marchisio, P. C. (1989). Ultrastructure and gold-immunolabelling of cell-substratum adhesions (podosomes) in RSV-transformed BHK cells. J. Cell Sci. *94*, 85–99.

Gimona, M., and Buccione, R. (2006). Adhesions that mediate invasion. Int. J. Biochem. Cell Biol. *38*, 1875–1892.

Gimona, M., Kaverina, I., Resch, G. P., Vignal, E., and Burgstaller, G. (2003). Calponin repeats regulate actin filament stability and formation of podosomes in smooth muscle cells. Mol. Biol. Cell *14*, 2482–2491.

Glading, A., Uberall, F., Keyse, S. M., Lauffenburger, D. A., and Wells, A. (2001). Membrane proximal ERK signaling is required for M-calpain activation downstream of epidermal growth factor receptor signaling. J. Biol. Chem. *276*, 23341–23348.

Hall, T. J., Schaeublin, M., and Missbach, M. (1994). Evidence that c-src is involved in the process of osteoclastic bone resorption. Biochem. Biophys. Res. Commun. *199*, 1237–1244.

Huang, C., Tandon, N. N., Greco, N. J., Ni, Y., Wang, T., and Zhan, X. (1997). Proteolysis of platelet cortactin by calpain. J. Biol. Chem. *272*, 19248–19252.

Jurdic, P., Saltel, F., Chabadel, A., and Destaing, O. (2006). Podosome and sealing zone: specificity of the osteoclast model. Eur. J. Cell Biol. *85*, 195–202.

Lee, E., and De Camilli, P. (2002). Dynamin at actin tails. Proc. Natl. Acad. Sci. USA *99*, 161–166.

Linder, S. (2007). The matrix corroded: podosomes and invadopodia in extracellular matrix degradation. Trends Cell Biol. *17*, 107–117.

Linder, S., and Aepfelbacher, M. (2003). Podosomes: adhesion hot-spots of invasive cells. Trends Cell Biol. *13*, 376–385.

Linder, S., Hufner, K., Wintergerst, U., and Aepfelbacher, M. (2000). Microtubule-dependent formation of podosomal adhesion structures in primary human macrophages. J. Cell Sci. *113*, 4165–4176.

Linder, S., and Kopp, P. (2005). Podosomes at a glance. J. Cell Sci. *118*, 2079–2082.

Linder, S., Nelson, D., Weiss, M., and Aepfelbacher, M. (1999). Wiskott-Aldrich syndrome protein regulates podosomes in primary human macrophages. Proc. Natl. Acad. Sci. USA *96*, 9648–9653.

Luxenburg, C., Parsons, J. T., Addadi, L., and Geiger, B. (2006). Involvement of the Src-cortactin pathway in podosome formation and turnover during polarization of cultured osteoclasts. J. Cell Sci. *119*, 4878–4888.

Marchisio, P. C., Bergui, L., Corbascio, G. C., Cremona, O., D'Urso, N., Schena, M., Tesio, L., and Caligaris-Cappio, F. (1988). Vinculin, talin, and integrins are localized at specific adhesion sites of malignant B lymphocytes. Blood *72*, 830–833.

Marchisio, P. C., Cirillo, D., Naldini, L., Primavera, M. V., Teti, A., and Zambonin-Zallone, A. (1984). Cell-substratum interaction of cultured avian osteoclasts is mediated by specific adhesion structures. J. Cell Biol. *99*, 1696–1705.

Marchisio, P. C., Cirillo, D., Teti, A., Zambonin-Zallone, A., and Tarone, G. (1987). Rous sarcoma virus-transformed fibroblasts and cells of monocytic origin display a peculiar dot-like organization of cytoskeletal proteins involved in microfilament-membrane interactions. Exp. Cell Res. *169*, 202–214.

McNiven, M. A., Baldassarre, M., and Buccione, R. (2004). The role of dynamin in the assembly and function of podosomes and invadopodia. Front. Biosci. *9*, 1944–1953.

Mizutani, K., Miki, H., He, H., Maruta, H., and Takenawa, T. (2002). Essential role of neural Wiskott-Aldrich syndrome protein in podosome formation and degradation of extracellular matrix in src-transformed fibroblasts. Cancer Res. *62*, 669–674.

Moreau, V., Tatin, F., Varon, C., and Genot, E. (2003). Actin can reorganize into podosomes in aortic endothelial cells, a process controlled by Cdc42 and RhoA. Mol. Cell. Biol. *23*, 6809–6822.

Mueller, S. C., and Chen, W. T. (1991). Cellular invasion into matrix beads: localization of beta 1 integrins and fibronectin to the invadopodia. J. Cell Sci. *99*, 213–225.

Mueller, S. C., Yeh, Y., and Chen, W. T. (1992). Tyrosine phosphorylation of membrane proteins mediates cellular invasion by transformed cells. J Cell Biol. *119*, 1309–1325.

Nakamura, K., Yano, H., Uchida, H., Hashimoto, S., Schaefer, E., and Sabe, H. (2000). Tyrosine phosphorylation of paxillin alpha is involved in temporospatial regulation of paxillin-containing focal adhesion formation and F-actin organization in motile cells. J. Biol. Chem. *275*, 27155–27164.

Ochoa, G. C. *et al*. (2000). A functional link between dynamin and the actin cytoskeleton at podosomes. J. Cell Biol. *150*, 377–389.

Petit, V., Boyer, B., Lentz, D., Turner, C. E., Thiery, J. P., and Valles, A. M. (2000). Phosphorylation of tyrosine residues 31 and 118 on paxillin regulates cell migration through an association with CRK in NBT-II cells. J. Cell Biol. *148*, 957–970.

Pfaff, M., and Jurdic, P. (2001). Podosomes in osteoclast-like cells: structural analysis and cooperative roles of paxillin, proline-rich tyrosine kinase 2 (Pyk2) and integrin alphaVbeta3. J. Cell Sci. *114*, 2775–2786.

Rodriguez, L. G., and Guan, J. L. (2005). 14-3-3 regulation of cell spreading and migration requires a functional amphipathic groove. J. Cell. Physiol. *202*, 285–294.

Salgia, R. *et al*. (1995). Molecular cloning of human paxillin, a focal adhesion protein phosphorylated by P210BCR/ABL. J. Biol. Chem. *270*, 5039–5047.

Schaller, M. D. (2001). Paxillin: a focal adhesion-associated adaptor protein. Oncogene *20*, 6459–6472.

Schaller, M. D., and Parsons, J. T. (1995). pp125FAK-dependent tyrosine phosphorylation of paxillin creates a high-affinity binding site for Crk. Mol. Cell. Biol. *15*, 2635–2645.

Tarone, G., Cirillo, D., Giancotti, F. G., Comoglio, P. M., and Marchisio, P. C. (1985). Rous sarcoma virus-transformed fibroblasts adhere primarily at discrete protrusions of the ventral membrane called podosomes. Exp. Cell Res. *159*, 141–157.

Tehrani, S., Faccio, R., Chandrasekar, I., Ross, F. P., and Cooper, J. A. (2006). Cortactin has an essential and specific role in osteoclast actin assembly. Mol. Biol. Cell *17*, 2882–2895.

Turner, C. E., Glenney, J. R., Jr., and Burridge, K. (1990). Paxillin: a new vinculin-binding protein present in focal adhesions. J. Cell Biol. *111*, 1059–1068.

Vindis, C., Teli, T., Cerretti, D. P., Turner, C. E., and Huynh-Do, U. (2004). EphB1-mediated cell migration requires the phosphorylation of paxillin at Tyr-31/Tyr-118. J. Biol. Chem. *279*, 27965–27970.

Webb, B. A., Jia, L., Eves, R., and Mak, A. S. (2007). Dissecting the functional domain requirements of cortactin in invadopodia formation. Eur. J. Cell Biol. *86*, 189–206.

Webb, D. J., Donais, K., Whitmore, L. A., Thomas, S. M., Turner, C. E., Parsons, J. T., and Horwitz, A. F. (2004). FAK-Src signalling through paxillin, ERK and MLCK regulates adhesion disassembly. Nat. Cell Biol. *6*, 154–161.

Westhoff, M. A., Serrels, B., Fincham, V. J., Frame, M. C., and Carragher, N. O. (2004). SRC-mediated phosphorylation of focal adhesion kinase couples actin and adhesion dynamics to survival signaling. Mol. Cell. Biol. *24*, 8113–8133.

Yamaguchi, H. *et al*. (2005). Molecular mechanisms of invadopodium formation: the role of the N-WASP-Arp2/3 complex pathway and cofilin. J. Cell Biol. *168*, 441–452.

Yoneda, T., Lowe, C., Lee, C. H., Gutierrez, G., Niewolna, M., Williams, P. J., Izbicka, E., Uehara, Y., and Mundy, G. R. (1993). Herbimycin A, a pp60c-src tyrosine kinase inhibitor, inhibits osteoclastic bone resorption in vitro and hypercalcemia in vivo. J. Clin. Invest. *91*, 2791–2795.

Zaidel-Bar, R., Milo, R., Kam, Z., and Geiger, B. (2007). A paxillin tyrosine phosphorylation switch regulates the assembly and form of cell-matrix adhesions. J. Cell Sci. *120*, 137–148.